# INERTIAL UPPER STAGE THREE-DIMENSIONAL THERMAL ANALYSIS*

I-Shih Chang
The Aerospace Corporation
El Segundo, California

ABSTRACT

An efficient technique for three-dimensional thermal modeling which involves automated pre-processing, analysis, and post-processing is discussed. The technique is based on a finite element method and computer-aided-design geometry modeling. The results obtained from thermal analysis are directly compatible with structural computational mesh without any interpolation. Numerical calculations are carried out for a three-dimensional convection heating fixture configuration from The Aerospace Corporation's Aerophysics Laboratory arc jet test and for an IUS SRM-2 full-scale titanium housing subject to an oxygen-acetylene torch heating performed at United Technologies Corporation's Chemical Systems Division. The computed temperature data are compared with those of thermocouple measurements. They are presented in three-dimensional colored temperature contours with enhanced temperature field visualization which provides designers with clear pictures of thermal penetration in three-dimensional objects.

## 1. INTRODUCTION

The Inertial Upper Stage (IUS) is used to put the large payloads into geosynchronous orbit. It consists of two solid rocket motor stages (SRM-1 and SRM-2) and an equipment support section containing the avionics necessary for guidance and control. Figure 1 shows the IUS configuration, and Figs. 2 and 3 depict SRM-1 and SRM-2 geometry. During the second IUS flight (IUS-1) on 4 April 1983, the full-loaded second stage rocket motor (SRM-2) experienced a thrust vector control anomaly at approximately 84 sec into the burn. The nominal total burn time for the SRM-2 is 105 sec. After extensive investigation by technical members from Boeing Aerospace Company (BAC), Chemical Systems Division (CSD) of United Technologies Corporation (UTC), NASA, the Air Force, and The Aerospace Corporation, in-flight loss of thrust vectoring capability for the IUS SRM-2 has been attributed to burst of the pressurized Techroll seal (TRS) on which the nozzle rides. Figure 4 is a detailed sketch of the SRM-2 nozzle block with the darkened area representing the TRS. The seal is filled with oil and forms a flexible cushion which bears against the nozzle but allows the nozzle to be gimballed. Rupture of the seal and depletion of the silicone oil contained therein would cause jamming of the nozzle gimbal mechanism. An overview of the IUS motor assembly, flight data, anomaly investigation, design enhancements and modifications, and motor test program has been presented by the motor contractor, CSD, and is given in Ref. 1.

From the thermocouple imbedded inside the titanium housing in the full-instrumented full-scale BS-1 (Baseline Small Motor No. 1) motor, which was statically tested successfully on 2 December 1983, it was observed that the peak measured temperature reached 800°F in the housing. This temperature was much higher than that predicted before the test. Inspection of the post-fire hardware revealed that the surface of the titanium housing forward of the shear lip was locally discolored. This indicated that combustion gas leaked through the nozzle thermal protection system and through the Grafoil seal port shown in Fig. 4 some time during motor firing and came in direct contact with the housing surface. A strong possibility then existed that IUS-1 suffered similar abnormal excessive heating to the SRM-2 Techroll housing (TRH) during the flight in April 1983. To investigate this scenario and to better understand the environment associated with direct combustion gas heating of the titanium housing, the Aerospace Aerophysics Laboratory conducted an argon arc jet heating test for a titanium plate, which was configured to simulate the SRM-2 housing shear lip area. In addition, full-scale IUS SRM-2 TRH inside diameter (ID) thermal tests were also conducted by CSD. The objectives of the tests were to gain a better insight into TRH thermal response and to determine TRS failure temperature under a severe combined heating and pressure load.

The three-dimensional (3-D) nature of locally heating the titanium housing of the TRS in the SRM-2 nozzle observed in the ground motor tests and postulated for the flight motor has served to emphasize the need for an efficient technique to perform 3-D thermal analyses. In particular, accurate prediction of TRS temperatures for the "worst case" Grafoil seal leak scenario has been hampered by the lack of such a technique. The "worst case" analyses were limited to two-dimensional (2-D) analyses because of well-known difficulties involved in modeling geometry in 3-D space, imposing tedious boundary conditions on a complicated 3-D surface, and interpreting massive 3-D data obtained from analysis.

*This study was supported by the Space Division, Air Force Systems Command under Contract No. F04701-83-C-0084. Approved for public release; distribution is unlimited.

In this paper, an efficient technique involving the use of PATRAN software (Ref. 2) at the Aerospace Computer-Aided-Engineering (CAE) facility for arbitrary 3-D geometry modeling and the finite element thermal analyzer in NASTRAN (NAsa STRuctural ANalysis computer program) (Ref. 3) for general 3-D thermal analysis is discussed. The technique has the following features:

- o Easy treatment of any arbitrary 3-D configuration
- o Applicability of steady or transient, linear or nonlinear problems
- o Capability of handling very general boundary conditions--radiation, convection, or direct heat flux input
- o Allowance for isotropic and anisotropic temperature-dependent thermal conductivity
- o No interpolation of output temperature data for structural analysis
- o Minimum effort for a complete thermal analysis--automated pre-processing, analysis, and post-processing procedure

The first application of the 3-D thermal modeling technique mentioned above to the SRM-2 titanium housing area is given in Ref. 4, which serves to illustrate and compare the results computed from 1-, 2-, and 3-D analyses under a very simple boundary condition: namely, direct combustion diffusion gas heating on the tip surface of titanium housing shear lip. The application of the 3-D thermal analysis technique to the Aerospace arc jet test configuration and to the CSD full-scale SRM-2 TRH ID torch test geometry mentioned above is explored in this study. The results of calculations are compared well with those of thermocouple measurements from the tests.

## 2. METHODOLOGY

The general theory for the finite element method of thermal analysis is given in NASTRAN's manual (Ref. 3). In summary, a general heat conduction equation

$$\rho c \frac{du}{dt} = \nabla \cdot (K \nabla u) + q_v ,$$

after applying the variational principle and constructing the finite element equations, takes the form

$$[B] \{\dot{u}\} + [K] \{u\} = \{P\} + \{N\}$$

which is globally very similar to the vibration equation for general transient structural analysis used in NASTRAN: namely

$$[M] \{\ddot{u}\} + [B] \{\dot{u}\} + [K] \{u\} = \{P\} + \{N\}$$

The NASTRAN Thermal Analyzer (NTA) takes advantage of some already developed structural algorithms for the thermal analysis. The mathematical analogy between the structural and thermal systems is as follows:

| Structural System | Symbol | Thermal System |
|---|---|---|
| displacement | u | temperature |
| velocity | $\dot{u}$ | rate change of temperature |
| acceleration | $\ddot{u}$ | -- |
| gradient | $\nabla u$ | temperature gradient |
| stiffness | K | conductance |
| damping | B | heat capacitance |
| mass | M | -- |
| applied force | P | thermal load |
| nonlinear force | N | nonlinear thermal load (radiation) |
| strain energy function | U | thermal potential function = $-(1/2) \int_v \tilde{q} \cdot \nabla u \, dv$ (where $\tilde{q}$ = heat flux density) |

The application of PATRAN software to geometry and finite element modeling, pre-processing, and analysis data post-processing is discussed in detail in Ref. 2. Figure 5 illustrates the operational procedure in thermal analysis, which would be the same in a structural analysis using NASTRAN or a similar finite element program.

## 3. 3-D THERMAL ANALYSIS FOR AEROSPACE ARC JET TEST CONFIGURATION

In order to establish the convection heating environment and to gain more confidence with 3-D thermal modeling, the analysis technique mentioned above is applied to an arc jet test configuration which was subject to a heating environment closely simulating diffusion gas heating on titantium housing in the BS-1 motor. The arc jet test was conducted at the Aerospace Aerophysics Laboratory (Ref. 5).

### 3.1 TEST CONFIGURATION

The arc jet convection heating test fixture and thermocouple placement in the titanium plate are illustrated in Figs. 6 and 7, respectively. Initially, the test assembly is at 70°F, and the test cell pressure is maintained at 0.0097 psia (0.5 torr). The argon jet flows through a 0.59 x 0.015-in. slot as shown in Fig. 6 at a mass flow rate of 0.0061 lb/sec with stagnation pressure at 90 psia and average recovery temperature at 3100°F. The total heating time of the arc jet is 31 sec.

### 3.2 GEOMETRY MODELING AND THERMAL BOUNDARY CONDITIONS

Based on the technique discussed above, the complete 3-D finite element geometry model obtained from PATRAN software at The Aerospace CAE facility is given in Fig. 8 for the heated surface view and in Fig. 9 for the backside surface view. It is an easy matter to generate an associated 2-D geometry model once the 3-D model has been created. Thus, the 2-D model of titanium plate, which can also be considered as the cross-sectional view of the 3-D model, is also created and illustrated in Fig. 10. The total number of nodal points is 1000 (648 elements) for the 3-D model and 100 (72 elements) for the 2-D model. Due to jet flow symmetry, only a half portion of the titanium plate is considered in this study. The nodal points of the computational mesh have been clustered near the plane of symmetry and near the shear lip area, in order to have better resolution of the temperature field with steep temperature gradient in these regions. In PATRAN, the nodal points clustering is carried out through the use of a nonuniform parameterization option for geometry modeling.

The titanium plate in the arc jet test is assumed to be insulated on all surfaces except the area exposed to the arc jet, which is shown in the 2-D view of Fig. 11. The exposed boundary surface is subject to convective heating. Mathematically, this means $-k(\partial T/\partial n)_w = h_c(T_g - T_w)$ on the heated surface. Here k is titanium conductivity, $h_c$ is the surface heat transfer coefficient, T is temperature, n is the coordinate normal to the surface, and the subscripts g and w indicate gas and wall, respectively. Intuitively, for this forced convection heating problem, one might be tempted to use an "open" jet impingement theory to estimate the convection heat transfer coefficient (htc) near the jet exit region between the argon jet and the titanium plate, with the downstream htc evaluated from a turbulent pipe flow equation. This htc distribution is shown in Fig. 11. Since one of the purposes of this study is to establish the correct convection heating environment from known measured responses of the thermocouples imbedded in the titanium plate, it does not matter what value of htc is used as an initial guess. Hence, the dashed curve obtained from the open jet impingement theory shown in Fig. 11 is used to start the numerical calculation. The heating rate along the direction normal to the symmetry plane is assumed to be at peak value on the titanium plate directly facing the slot and to fall off rapidly beyond the edge of the slot. This would follow the same trend as the heating rate curve shown in Fig. 11.

### 3.3 COMPARISON OF COMPUTATIONAL RESULTS WITH TEST DATA

With the argon jet temperature history shown in Fig. 12 as the driving thermal potential and the surface film thermal conductance evaluated from the dashed curve in Fig. 11, the computed temperatures at thermocouple locations (4) and (2) are given as dashed curves in Figs. 12 and 13, respectively. The measured temperatures from thermocouples (4) and (2) are also shown in Figs. 12 and 13 for comparison. At the end of 31-sec heating, the predicted temperature based on the "open" jet impingement theory is 2406°F at location (4) and 1308°F at location (2), whereas the measured values are 1100°F and 830°F, respectively. The use of htc from the "open" jet impingement theory drastically overpredicts titanium temperatures at locations (4) and (2). This indicates inadequacy of the direct application of the "open" jet theory to the test configuration with a confined region for jet flow.

A trial and error method is then applied to adjust the surface htc in order to gain a better match between the predicted temperature and measured value. The argon jet gas temperature drops only 100°F from entrance to exit along the flow direction on the symmetry plane from a one-dimensional flow tube analysis. The effect of spatial variation of gas jet temperature is implicitly taken into account through the htc distribution. The final htc curve thus obtained is shown as a solid curve in Fig. 11. It reveals a peak htc at the location of jet impingement of $2.0 \times 10^{-4}$ Btu/in.$^2$-sec-°F, which is more than an order of magnitude smaller than $2.52 \times 10^{-3}$ Btu/in.$^2$-sec-°F from the "open" jet impingement theory.

The solid curves in Figs. 12 through 14 are the computed temperatures obtained from imposing this new correlated htc distribution on the titanium heated surface; they compare favorably with the measured temperatures from thermocouple readings. Note that thermocouple (1) measured data are not available and thermocouple (3) shows higher temperature than (5), implying possible loss of contact between imbedded thermocouples and the titanium plate.

The maximum difference between the computed temperature and the measured data is less than 10 percent at all locations where thermocouple readings are available. The main reason for the difference lies in the fact that the gas jet temperature is "estimated" and could be conservative. If, for example, the gas temperature is reduced somewhat, and the htc is slightly increased (to the order of $3.0 \times 10^{-4}$ Btu/in.$^2$-sec-°F), better agreement between the computed temperature and measured value at thermocouple locations (4) and (2) could be obtained. The present analysis, however, uses the gas temperature as supplied by the Aerospace Aerophysics Laboratory and makes no attempt to modify it. The requirement of constant titanium specific heat (0.16 Btu/lb-°F) in the thermal model using the NTA computer program (Ref. 3) can also introduce some variation of the computed temperature from that of the test. Finally, the computed 3-D temperature contour is given in Fig. 15 for the heated surface view and in Fig. 16 for the backside surface view. Since it is a simple matter to analyze a 2-D problem, once the associated 3-D thermal analysis has been completed, the 2-D model shown in Fig. 10 is also analyzed. Figure 17 illustrates the computed temperature contour for the 2-D model using the same axial heat transfer coefficient distribution (see Fig. 11). The difference between the computed results from 2-D and 3-D can be visually observed from these temperature contours. The 3-D contours shown in Figs. 15 and 16 clearly illustrate the computed 3-D temperature distribution in the titanium plate, including the region forward of the shear lip where no measured data are available. The computation time for the thermal analysis is 75.3 sec for the 3-D model and 9.8 sec for the 2-D model on a Cyber 176 machine located at The Aerospace Corporation.

## 4. THREE-DIMENSIONAL THERMAL ANALYSIS FOR CSD SRM-2 TRH TORCH HEATING TEST

Hypothesizing that the IUS-1 SRM-2 control anomaly was the result of TRS failure due to overheating of the titanium housing by combustion diffusion gas leaking through the Grafoil seal, CSD, the IUS motor contractor, conducted thermal tests. These tests locally heated the shear lip area of a full-scale SRM-2 titanium housing with an oxygen-acetylene torch flame. The heating rate was calibrated at the level which closely simulated the peak heating rate calculated from the DS-1 (Development Small Motor No. 1) (Ref. 6) static test data; it represented the most severe heating environment in the shear lip area that ever occurred in the IUS motor development and qualification program. A series of ID heating tests have been performed by CSD. The test data used for the present 3-D thermal analysis comparison are obtained from ID heating test No. 3 with TRS internal pressure set at 200 psia and torch flame heating rate calibrated at 0.36 Btu/in.$^2$-sec with a water-cooled Hycal Asymtatic calorimeter. The estimated flame core diameter is approximately 1 in. ∿ 1-1/4 in.. The total heating time until TRS collapsed was 80 sec.

### 4.1 TEST APPARATUS

The ID heating test apparatus is shown in Fig. 18 (excerpted from Ref. 1) by courtesy of C. A. Chase of CSD. The TRS was maintained at pre-established pressure by connecting the TRH silicone oil fill/bleed port to a bladder-like accumulator, which contained silicone oil and was pressurized by nitrogen. An oxygen (∿ 10 psia) -acetylene (∿ 5 psia) torch nozzle was placed near the titanium housing with a remote-controlled spark generator placed nearby for ignition. Fiber frax insulation material was used to protect thermocouple lead wires and prevent the torch flame from spreading into the TRH inner convolute area. The thermocouples were placed in the titanium housing and on the interface between the housing and the TRS (see Fig. 19).

### 4.2 GEOMETRY MODELING AND THERMAL BOUNDARY CONDITIONS

The complete 3-D finite element geometry model generated from the method mentioned above is given in Fig. 20 for the heated surface view and in Fig. 21 for the backside surface view. The associated 2-D cross-sectional view at the plane of symmetry is given in Fig. 22, which shows that the model considers a detailed geometry of TRS (0.010 in. neoprene rubber + 0.025 in. Kevlar + 0.040 in. neoprene rubber) and a 0.2-in. thick silicone oil in addition to the titanium housing

and the gib ring. The total number of nodal points is 2392 (1800 elements) for the 3-D model and 184 (150 elements) for the 2-D model. Due to assumed torch flame heating geometry, only a half portion of the titanium housing with a 45° circumferential region in the 3-D model is considered in this study. The nodal points of the computational mesh have been clustered near the plane of symmetry and near the shear lip to catch any steep temperature gradient in this area. The TRH is considered to be insulated on the surface, except on the area exposed to the torch flame. The pretest estimated heat transfer coefficient is $1.29 \times 10^{-4}$ Btu/in.$^2$-sec-°F which is used to start the iterative calculation for the heating environment through the best match with the thermocouple data. The torch flame gas temperature was measured from a Tungsten-Rhenium thermocouple and is given in Fig. 23. Note that the gib ring was not present in the torch test, whereas in the present thermal models, which are prepared for a complete SRM-2 TRH analysis, the gib ring is included.

## 4.3 COMPARISON OF COMPUTATIONAL RESULTS WITH TEST DATA

To attain a good match between the predicted temperature from the analysis and the thermocouple readings from the test, the heat transfer coefficient was found to be close to the axial distribution shown in Fig. 24, which illustrates a peak value of $1.70 \times 10^{-4}$ Btu/in.$^2$-sec-°F at the flame impingement center. The htc distribution along the azimuthal direction follows the same trend as that indicated in Fig. 24. Comparisons of the computed temperature with thermocouple data are given in Fig. 25 for TH1, TH2, TH14, and TH15 and in Fig. 26 for TH7 through TH11. Since most of the thermal analyses carried out by agencies involved in the IUS anomaly study have been restricted to either 1-D or 2-D analyses, it is interesting to investigate how much deviation from 3-D results one could expect from 1-D or 2-D analyses. For the present torch test, for example, a 1-D analysis considering a peak htc $1.70 \times 10^{-4}$ Btu/in.$^2$-sec-°F through the flame center station would give a temperature 1860°F at the TH13 location at the time of TRS rupture as shown in Fig. 27. A 2-D analysis considering axial and radial heat flux without circumferential heat relief and using the same htc distribution shown in Fig. 24 would result in a temperature 1480°F at the TH13 location. The 3-D analysis, however, "predicts" a temperature 1240°F, which is very close to the measured temperature 1210°F from the TH13 at the end of 80-sec heating. Therefore, it is misleading to use 1-D or 2-D results to establish the TRS failure temperature when the actual heating environment is 3-D in nature.

The computed 3-D temperature contour is given in Fig. 28 for the heated surface view and in Fig. 29 for the backside surface view. The associated temperature contour for the 2-D model is shown in Fig. 30. Note that this 2-D result is not the symmetry plane temperature distribution from 3-D analysis. Rather, it is a separate analysis using the htc distribution in Fig. 24 and the 2-D geometry model in Fig. 22.

One might wonder what the 3-D temperature distribution was in TRS, especially in load-carrying Kevlar layers, at the time of TRS rupture from this torch heating test. A large number of thermocouples need to be buried on the interface between TRS and the titanium housing wall in order to obtain such information from the torch heating test, which is both costly and time-consuming. In the present study, post-processing of analysis data is made easy through the use of the PATRAN post-processing routine which allows data associated with each component to be extracted separately from the complete model. In this instance, the Kevlar temperature data can be viewed independently from the complete 3-D finite element model. The 3-D temperature distribution on the hot side of Kevlar layers is shown in Fig. 31 and on the cold side in Fig. 32. This information is useful for the structures people to evaluate allowable Kevlar thermal strength for design improvements. The machine time for geometry and finite element modeling using PATRAN is 3 hr for 3-D and 5 min for 2-D on a VAX 11/780. The computation time for thermal analysis using NASTRAN is 305 sec for the 3-D model and 15 sec for the 2-D model on a Cyber 176 machine.

# 5. CONCLUSIONS

An efficient technique for general 3-D thermal modeling has been discussed. Correct heating rate distributions for both the arc jet test configuration from the Aerospace Aerophysics Laboratory and the SRM-2 TRH torch heating test at CSD have been established through the use of the present 3-D thermal analysis technique. The study showed that heat transfer coefficients predicted from the "open" jet impingement theory are far too conservative for the confined region encountered in the case of gas leaking and titanium plate heating. The study also showed that use of a 1-D or 2-D model to represent a 3-D configuration under a localized heating condition could lead to unrealistic results and conclusions. Despite the limitation of constant specific heat for materials involved in NASTRAN Thermal Analysis Modeling, the results obtained from the present analysis technique agree well with the measured thermocouple data; the maximum difference is less than 10 percent at all thermocouple locations. The colored temperature contours from post-processing of analysis results provide designers with clear pictures of thermal penetration in 3-D objects.

## REFERENCES


1. Chase, C. A., North, D. A., "IUS Propulsion Status," AIAA Paper 84-1192, Revision A, June 1984.

2. "PATRAN-G User's Manual," PDA Engineering, 1982.

3. MacNeal, Richard H., (ed.), "The NASTRAN Theoretical Manual," NASA SP-221, December 1972.

4. Chang, I-Shih, "IUS Three-Dimensional Thermal Analysis--SRM-2 Titanium Housing Sample Calculation," Aerospace Report No. TOR-0084(4464-02)-1, July 1984.

5. Private communication with D. J. Spencer, The Aerospace Corporation's Aerophysics Laboratory.

6. "IUS Full-scale Development Program DS-1 Final Test Report," CSD 5011-79-300, Revision A, Chemical Systems Division of United Technologies Corporation, 1979.


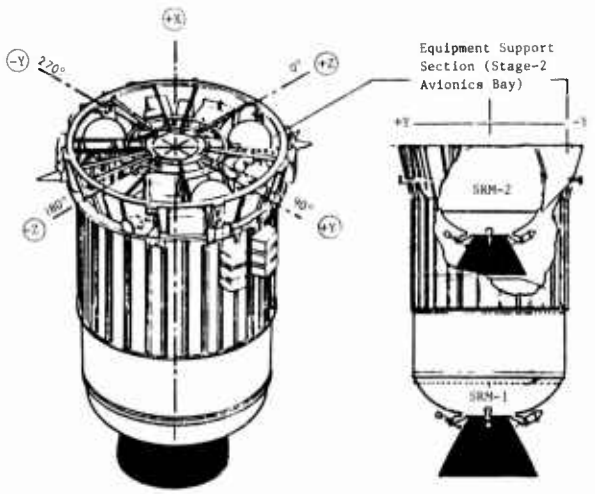


Fig. 1. IUS Configuration

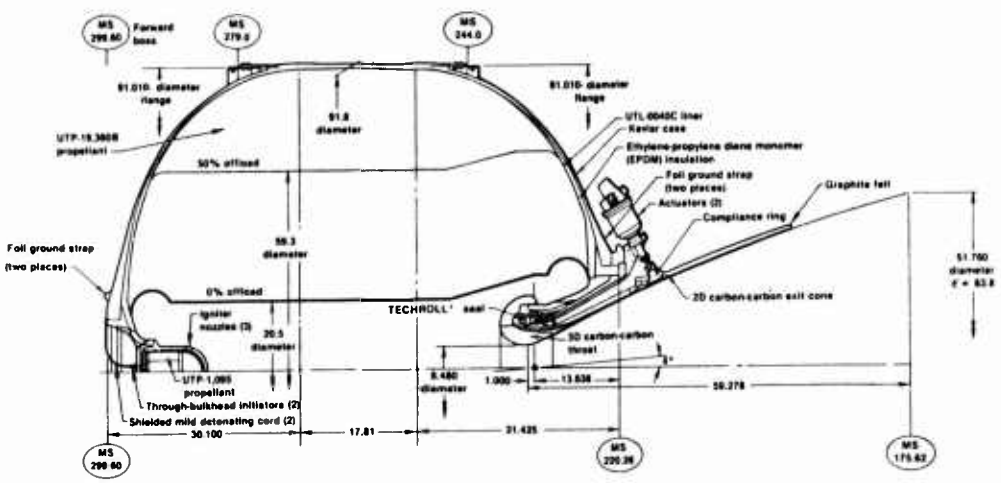


Fig. 2. SRM-1 Motor Assembly

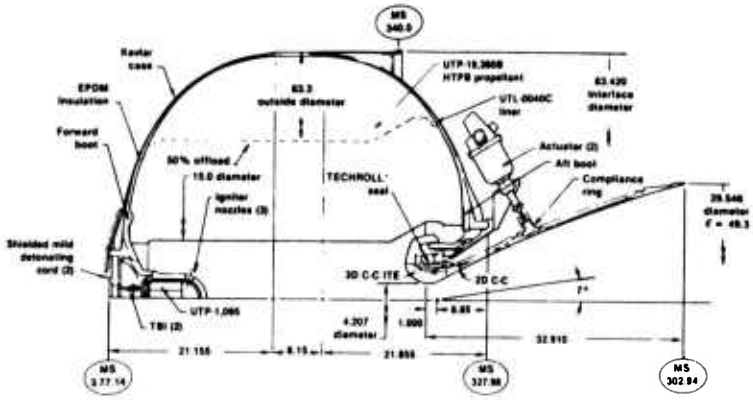

Fig. 3. SRM-2 Motor Assembly

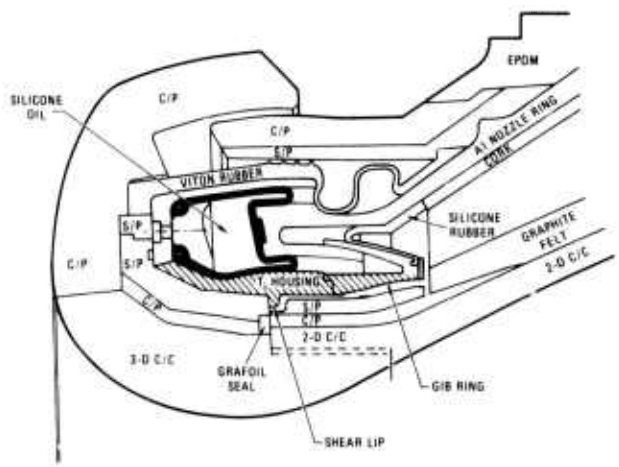


Fig. 4. IUS SRM-2 Nozzle and Exit Cone

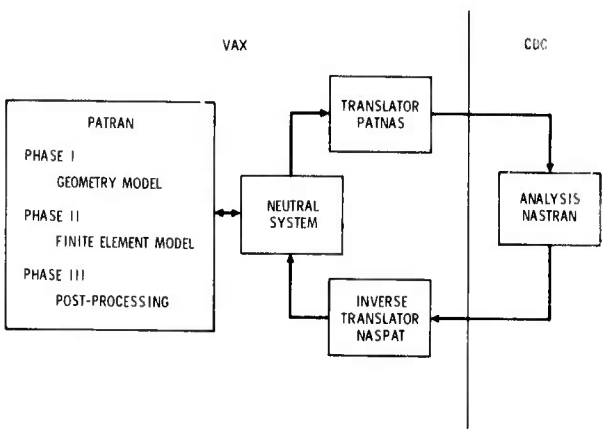


Fig. 5. Typical Thermal Analysis Operation

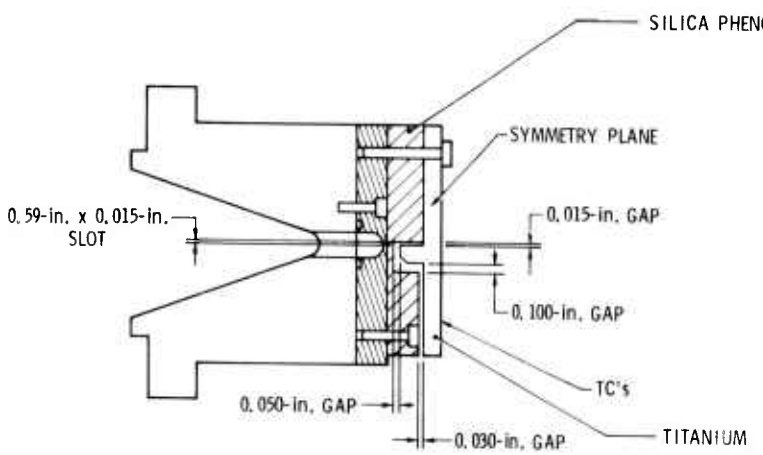


Fig. 6. Arc Jet Test Fixture Configuration

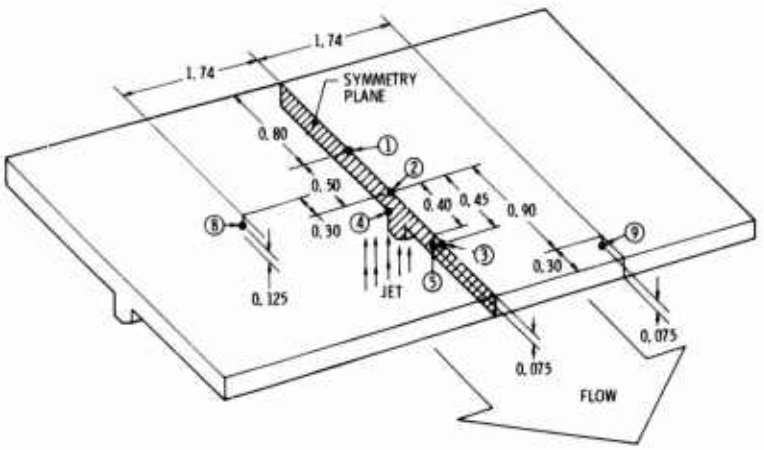


Fig. 7. Thermocouple Placement (denoted by circled numbers)

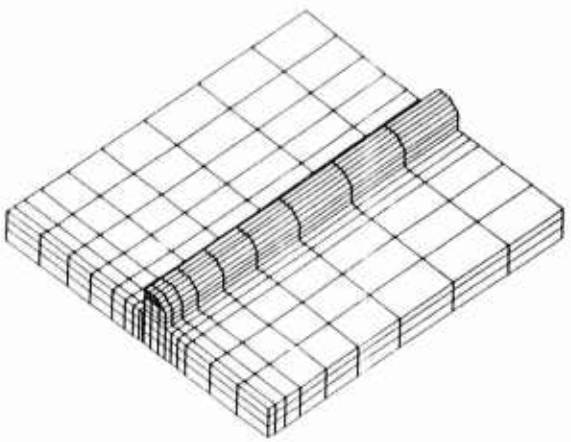

Fig. 8. 3-D Finite Element Thermal Model for Arc Jet Test Configuration: Heated Surface View

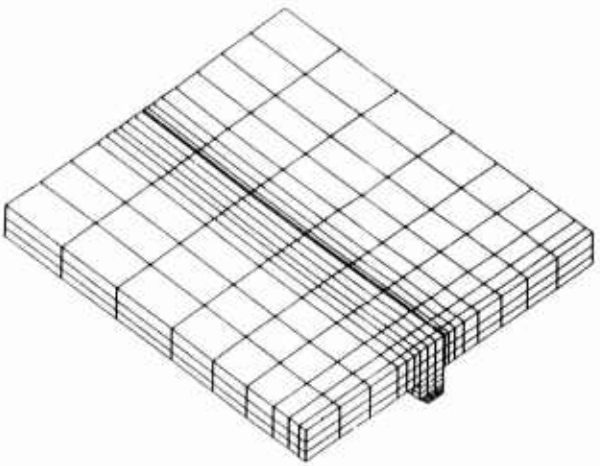

Fig. 9. 3-D Finite Element Thermal Model for Arc Jet Test Configuration: Backside Surface View

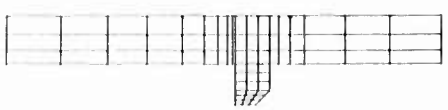

Fig. 10. 2-D Finite Element Thermal Model for Arc Jet Test Configuration

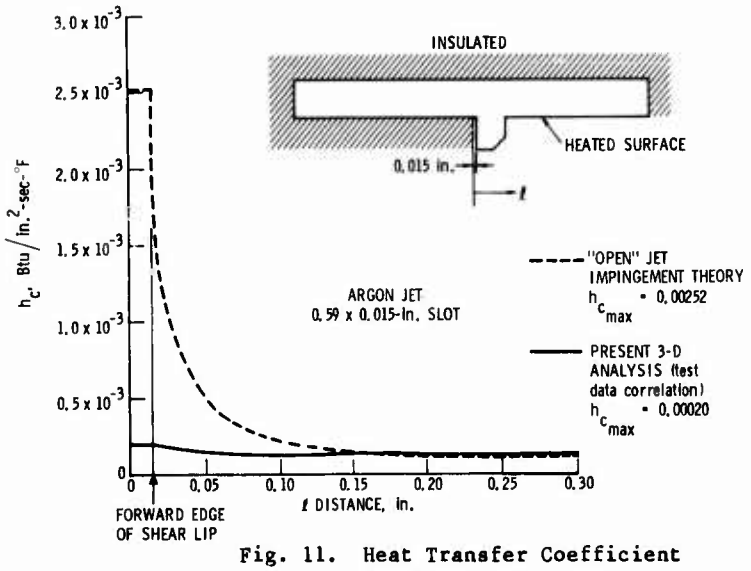


Fig. 11. Heat Transfer Coefficient for Arc Jet Test

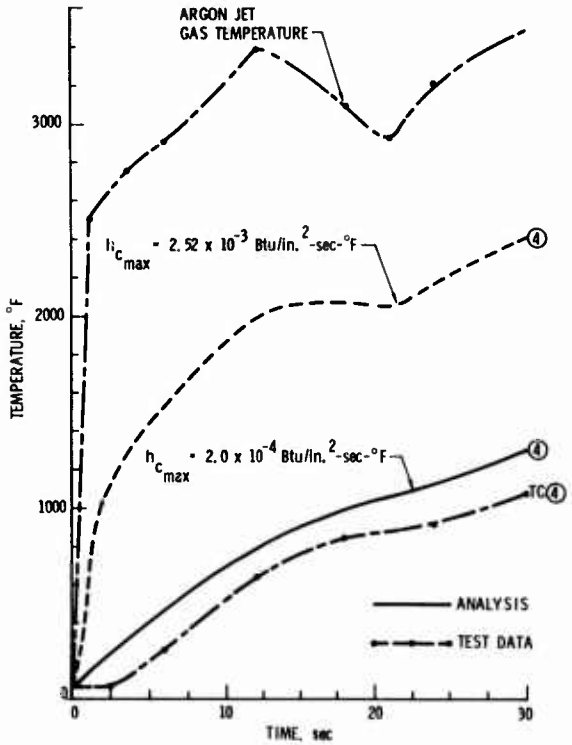


Fig. 12. Comparison of Analysis Results and Measured Data at TC ④

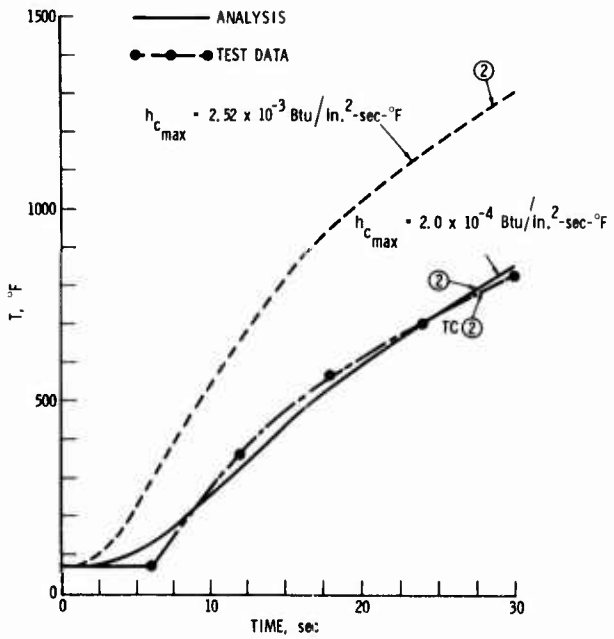


Fig. 13. Comparison of Analysis Results and Measured Data at TC ②

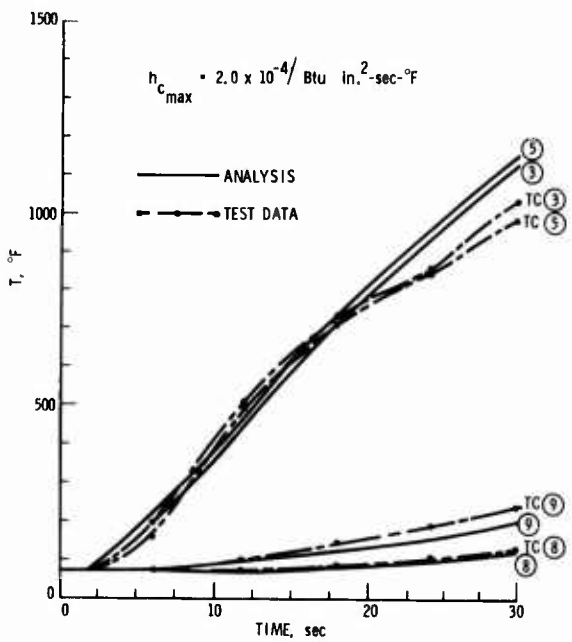


Fig. 14. Comparison of Analysis Results and Measured Data at TC ③ ⑤ ⑧ ⑨

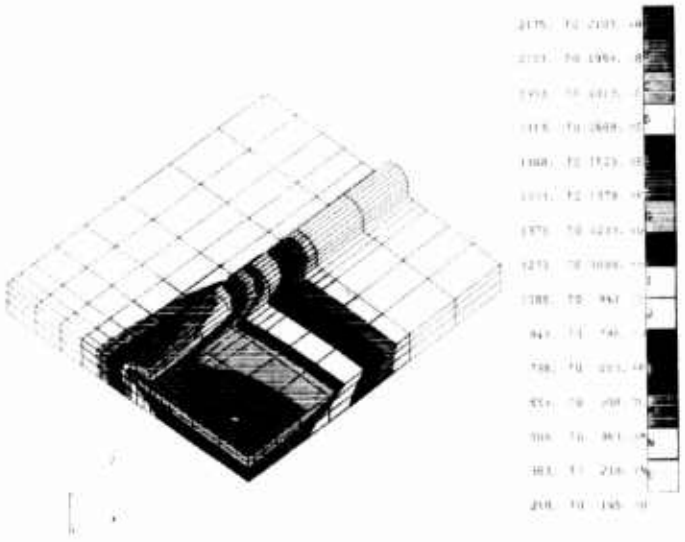

Fig. 15. 3-D Temperature Contour for Titanium Plate in Arc Jet Test: Heated Surface View

(original figures of temperature contours are in color)

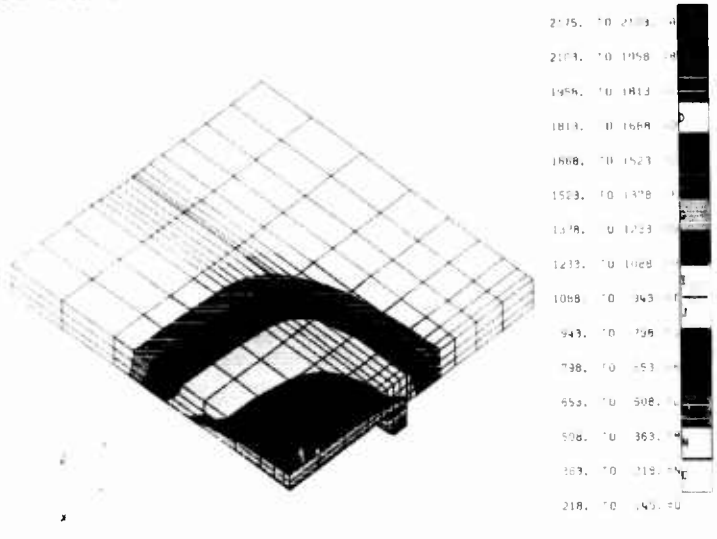

Fig. 16. 3-D Temperature Contour for Titanium Plate in Arc Jet Test: Backside Surface View

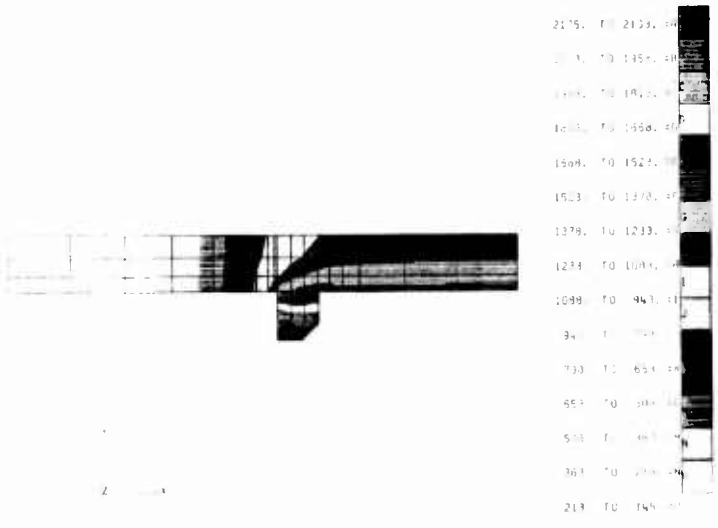

Fig. 17. 2-D Temperature Contour for Titanium Plate in Arc Jet Test

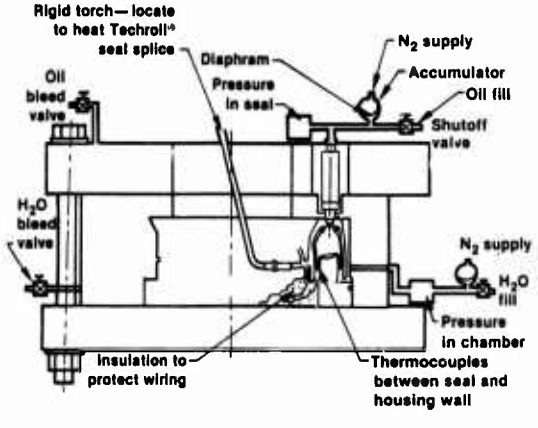


Fig. 18. Techroll Seal Inner Convolute Heating Test Setup

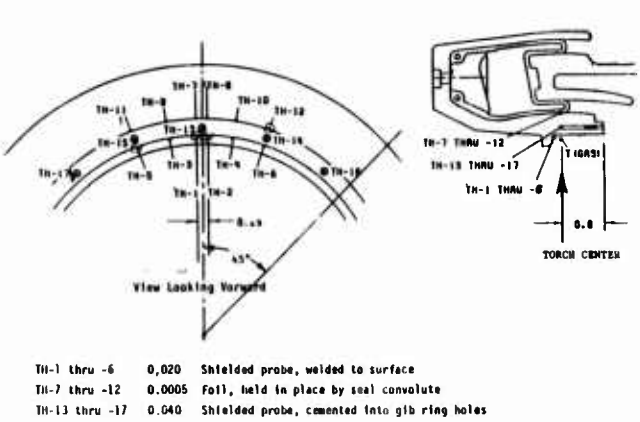


| | | |
|---|---|---|
| TH-1 thru -6 | 0.020 | Shielded probe, welded to surface |
| TH-7 thru -12 | 0.0005 | Foil, held in place by seal convolute |
| TH-13 thru -17 | 0.040 | Shielded probe, cemented into gib ring holes |

Fig. 19. Third I.D. Torch Test TRH Thermocouple Locations

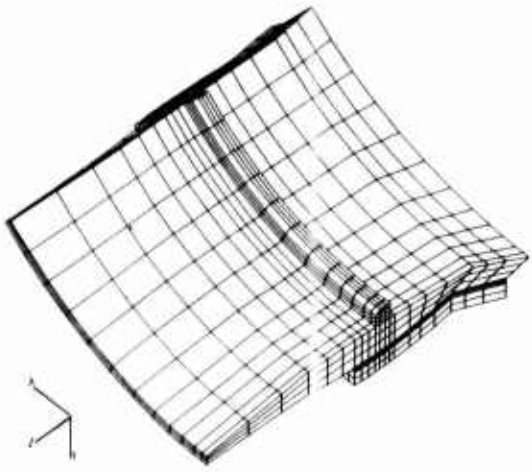

Fig. 20. 3-D SRM-2 TRH Finite Element Thermal Model: Heated Surface View

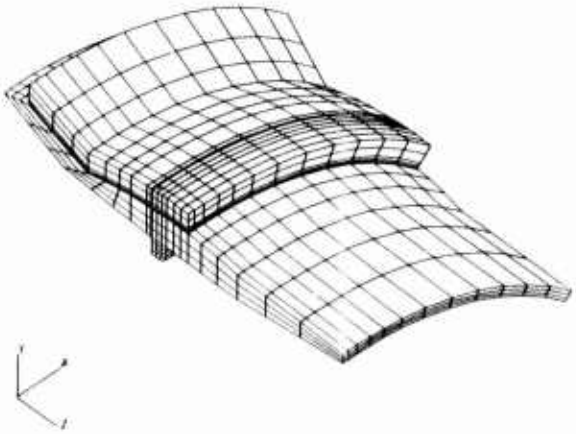

Fig. 21. 3-D SRM-2 TRH Finite Element Thermal Model: Backside Surface View

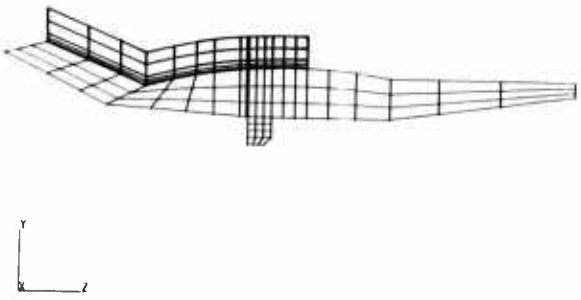

Fig. 22. 2-D SRM-2 TRH Finite Element Thermal Model

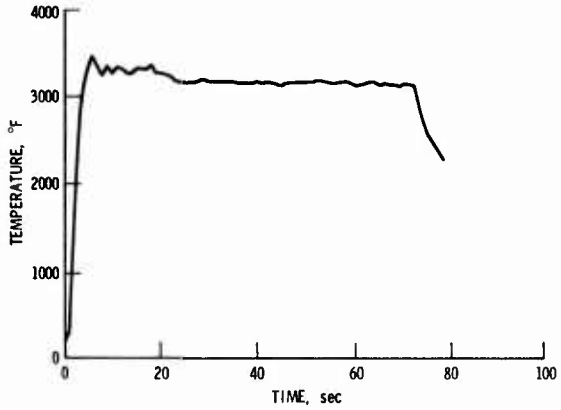


Fig. 23. Torch Flame Gas Temperature

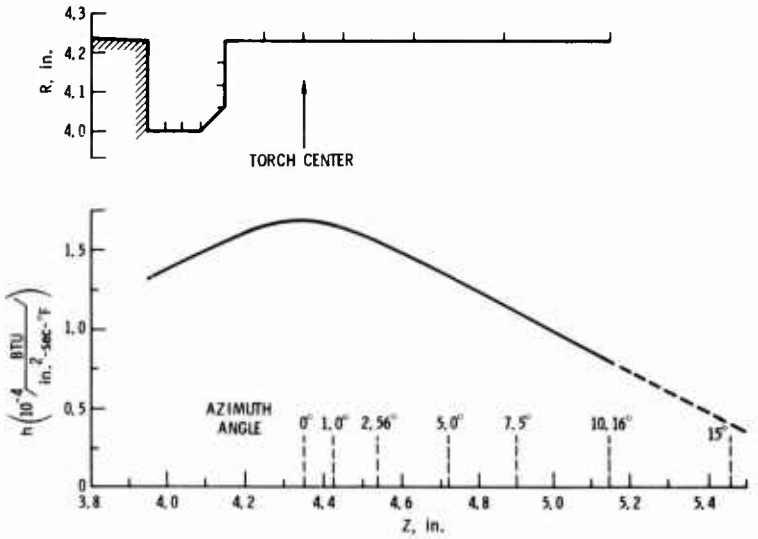


Fig. 24. SRM-2 TRH Heat Transfer Coefficient for Third I.D. Torch Test

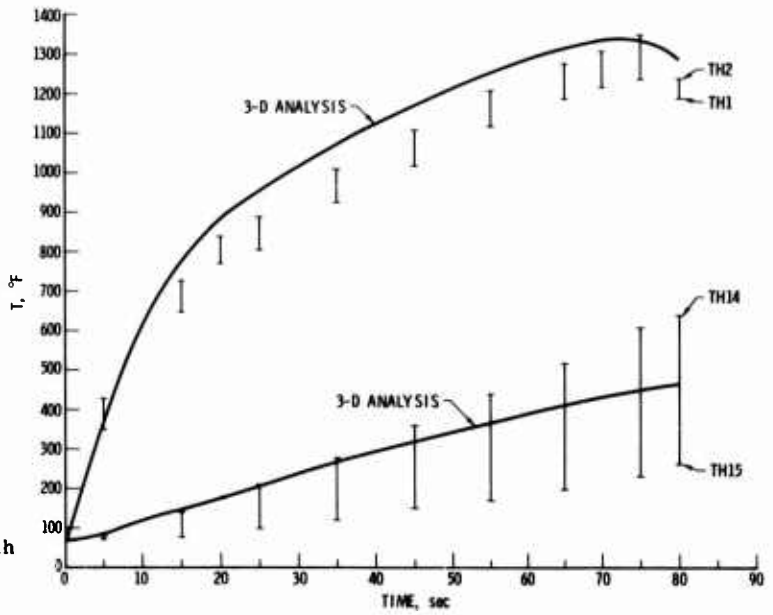


Fig. 25. Comparison of 3-D SRM-2 TRH Analysis Results with TH1, TH2, TH14, TH15 (third I.D. torch test)

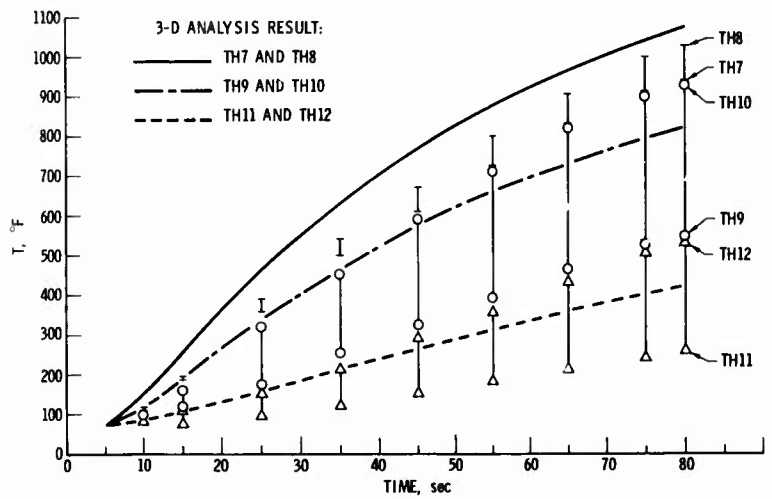


Fig. 26. Comparison of 3-D SRM-2 TRH Analysis Results with TH7 - TH12 (third I.D. torch test)

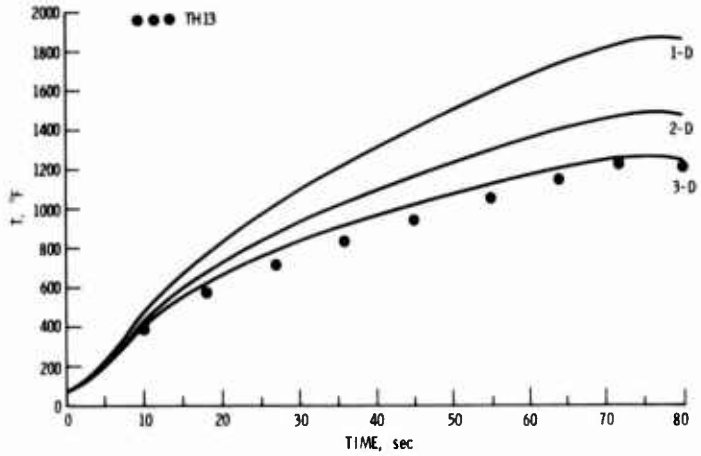


Fig. 27. Comparison of SRM-2 TRH Analysis Results with TH13 (third I.D. torch test)

(original figures of temperature contours are in color)

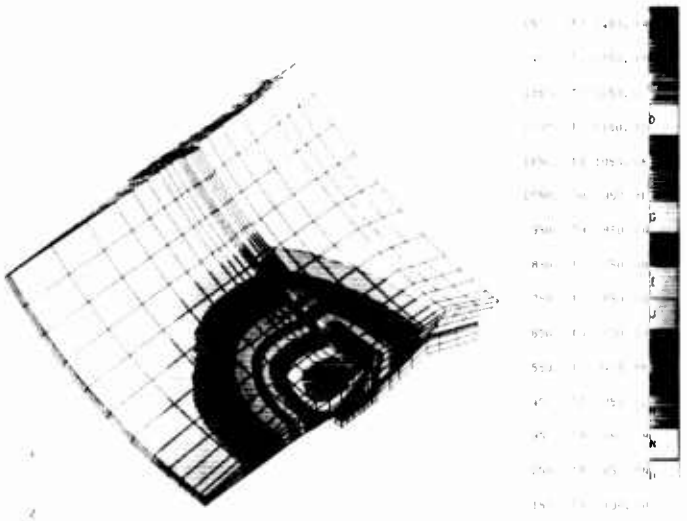

Fig. 28. 3-D Temperature Contour for SRM-2 TRH in Torch Heating Test: Heated Surface View

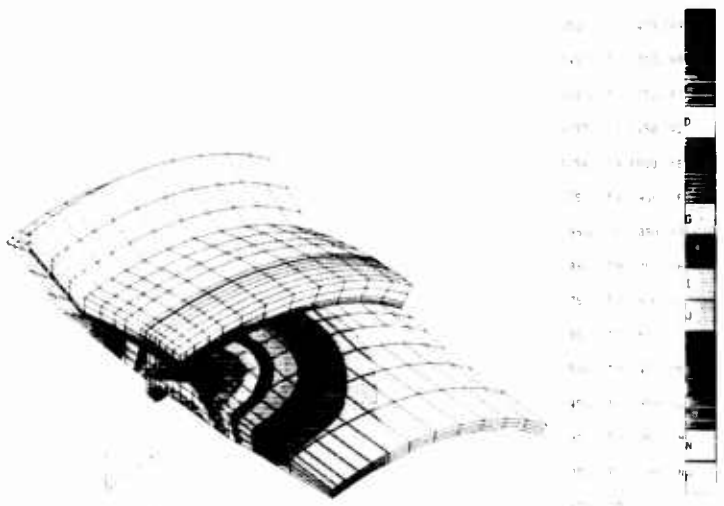

Fig. 29. 3-D Temperature Contour for SRM-2 in Torch Heating Test: Backside Surface View

(original figures are in color)

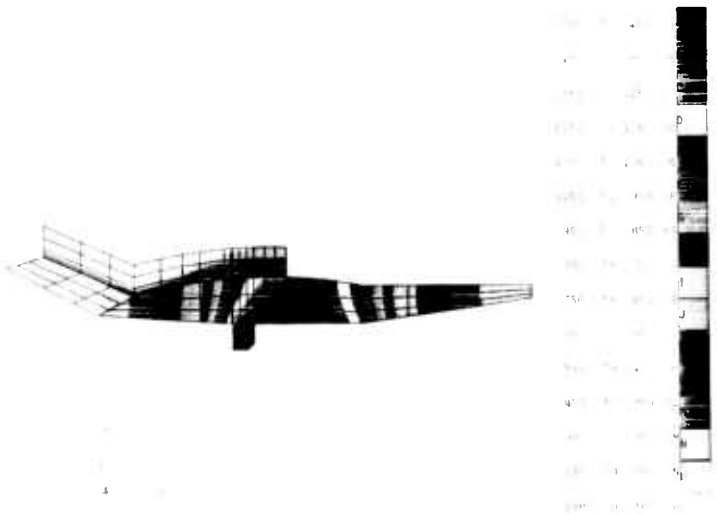

Fig. 30. 2-D Temperature Contour for SRM-2 TRH in Torch Heating Test

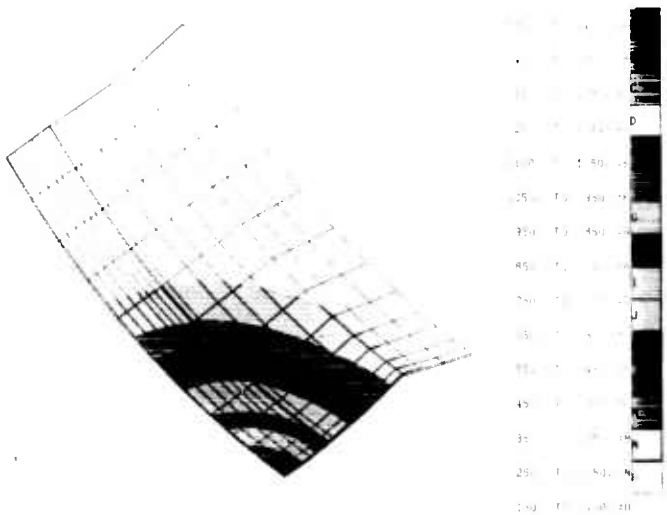

Fig. 31. 3-D Temperature Contour for Kevlar Layers in Torch Heating Test: Hot Side

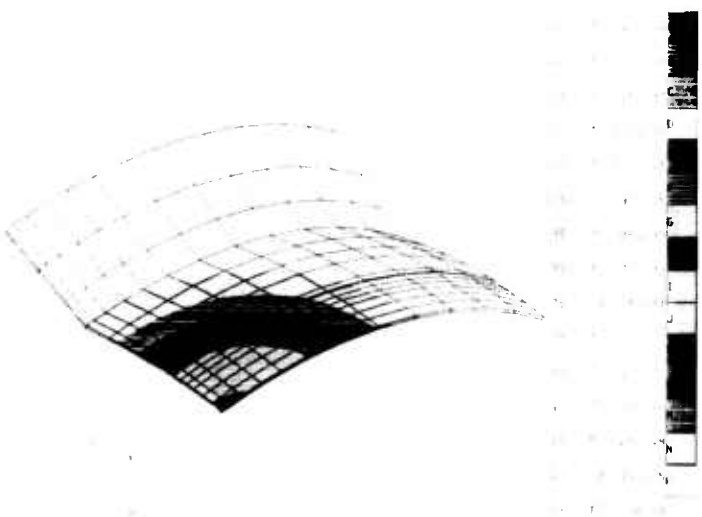

Fig. 32. 3-D Temperature Contour for Kevlar Layers in Torch Heating Test: Cold Side